Scale effects and the formation of polarization vortices in tetragonal ferroelectrics

Cite as: Appl. Phys. Lett. **106**, 092906 (2015); https://doi.org/10.1063/1.4913917
Submitted: 19 January 2015 . Accepted: 19 February 2015 . Published Online: 03 March 2015

Ananya Renuka Balakrishna, and John E. Huber

Scale effects and the formation of polarization vortices in tetragonal ferroelectrics

Ananya Renuka Balakrishna and John E. Huber[a)]
Department of Engineering Science, University of Oxford, Oxford OX1 3PJ, United Kingdom

(Received 19 January 2015; accepted 19 February 2015; published online 3 March 2015)

Vortices consisting of 90° quadrant domains are rarely observed in ferroelectrics. Although experiments show polarization flux closures with stripe domains, it is as yet unclear why pure single vortices are not commonly observed. Here, we model and explore the energy of polarization patterns with vortex and stripe domains, formed on the square cross-section of a barium titanate nanowire. Using phase-field simulations, we calculate the associated energy of polarization patterns as a function of nanowire width. Further, we demonstrate the effects of surface energy and electrical boundary conditions on equilibrium polarization patterns. The minimum energy equilibrium polarization pattern for each combination of surface energy and nanowire width is mapped for both open- and short-circuit boundary conditions. The results indicate a narrow range of conditions where single vortices are energetically favorable: nanowire widths less than about 30 nm, open-circuit boundary condition, and surface energy of less than 4 N/m. Short-circuit boundary conditions tend to favor the formation of a monodomain, while surface energy greater than 4 N/m can lead to the formation of complex domain patterns or loss of ferroelectricity. The length scale at which a polarization vortex is energetically favorable is smaller than the typical size of nanoparticle in recent experimental studies. The present work provides insight into the effects of scaling, surface energy, and electrical boundary conditions on the formation of polarization patterns. © *2015 AIP Publishing LLC*.
[http://dx.doi.org/10.1063/1.4913917]

Although vortices of magnetic domains have been experimentally observed in ferromagnets,[1–5] it is intriguing to note that the analogous simple polarization vortices are not seen in ferroelectrics. Models such as the time-dependent Ginzburg-Landau theory suggest that polarization vortices should form under certain conditions.[6–9]

Polarization vortices possess tremendous potential for the design of nanoscale devices such as memory elements[10–13] and transducers.[6,14,15] With the progressive miniaturization of electronics, the functional properties of ferroelectric domain patterns are of increasing importance.[16–20] Hence, much current research is directed towards finding polarization vortices and studying their nanoscale properties in detail.[21–31]

Polarization flux closures in the form of bundles of 90° stripe domains oriented to form a vortex have been imaged by McGilly and Gregg in $PbZr_{(0.42)}Ti_{(0.58)}O_3$ nanodots.[25] Similar stable flux closures have been observed by McQuaid *et al.* in $BaTiO_3$.[28] However, these flux-closures consist of 90° stripe domains[23,30] and so differ from the classic polarization vortex consisting of 90° quadrant domains, which is well-known in ferromagnetic materials.[32,33] Polarization vortex patterns consisting of dipole flux closures[26,28] or quadrupole chains[26] have been observed. However, these vortices have 180° domain walls at their core and so differ from the classic polarization vortex in small particles as predicted by Kittel.[1] Although the direct observation of polarization rotation which facilitates the formation of a vortex has been established,[24] the classic vortex polarization pattern continues to be elusive.[32] This leads us to consider the question—Why are these polarization vortices not seen in experiments?

In the present work, a $BaTiO_3$ nanowire in the tetragonal phase, with square cross-section, is modelled in isothermal conditions. The wire is assumed to extend indefinitely out of the model plane, such that plane strain and plane electric field conditions apply. Minimum cross-sectional widths of 20 nm were considered, noting that ferroelectricity has been observed in $BaTiO_3$ structures from a few nanometers in size upwards.[34–36] The wire is assumed to be simply supported, with traction free surfaces. We consider two distinct electrical boundary conditions: open- and short-circuit, by applying zero normal component of electric displacement and zero voltage boundary conditions, respectively.

A phase-field model previously developed by Landis and co-workers[37–39] calibrated for $BaTiO_3$ is used to find equilibrium states. This model has been applied as a design tool[6,11] and to study domain wall interactions in ferroelectrics.[37,38] The model describes the Helmholtz free energy, ψ as a function of polarization, P_i, which is the order parameter, strain, ε_{ij} and electric displacement, D_i

$$\psi = \psi_g + \psi_d, \tag{1}$$

$$\psi_g = \frac{1}{2} a_{ijkl} P_{i,j} P_{k,l}, \tag{2}$$

$$\begin{aligned}\psi_d = {} & \frac{1}{2}\bar{a}_{ij}P_iP_j + \frac{1}{4}\bar{\bar{a}}_{ijkl}P_iP_jP_kP_l \\ & + \frac{1}{6}\bar{\bar{\bar{a}}}_{ijklmn}P_iP_jP_kP_lP_mP_n + \frac{1}{8}\bar{\bar{\bar{\bar{a}}}}_{ijklmnrs}P_iP_jP_kP_lP_mP_nP_rP_s \\ & + b_{ijkl}\varepsilon_{ij}P_kP_l + \frac{1}{2}c_{ijkl}\varepsilon_{ij}\varepsilon_{kl} + \frac{1}{2}f_{ijklmn}\varepsilon_{ij}\varepsilon_{kl}P_mP_n \\ & + \frac{1}{2}g_{ijklmn}\varepsilon_{ij}P_kP_lP_mP_n + \frac{1}{2\kappa_0}(D_i - P_i)(D_i - P_i).\end{aligned} \tag{3}$$

[a)]Electronic mail: john.huber@eng.ox.ac.uk

The form of Eqs. (1)–(3) is identical to that in the work of Landis and co-workers,[37–39] where the detailed meaning of the specific terms and material properties are explained. For our purposes, we note that the gradient energy, ψ_g, includes energy due to polarization variation at domain walls or surfaces. The domain energy, ψ_d, accounts for the elastic, piezoelectric, and dielectric energy due to distortion away from the spontaneously polarized state. The domain evolution follows a generalized Ginzburg-Landau equation[37]

$$\left(\frac{\partial \psi}{\partial P_{i,j}}\right)_{,j} - \frac{\partial \psi}{\partial P_i} = \beta \dot{P}_i, \tag{4}$$

where β is the polarization viscosity, which was controlled as a relaxation parameter in the simulation to allow equilibrium states with $\beta = 0$ to be found. In the simulation, the polarization vector is constrained to lie in-plane with no other boundary conditions applied; it is governed by Eq. (4).

The phase-field model is solved using finite element methods with the element size chosen such that a 180° domain wall spans four elements. The nodal displacements enable the strain and polarization gradient to be computed; hence, the energy density was found from Eqs. (1)–(3).

To identify commonly occurring domain arrangements, the initial state of the model was set by assigning random polarization values, $\frac{-P_0}{2} \le P_i \le \frac{P_0}{2}$, at each node. Wire cross-sections in the size range $20\,\text{nm} \le L \le 40\,\text{nm}$ were simulated. From this random starting state, the simulation converged on equilibrium states, which frequently resulted in one of the three types of domain arrangement shown in Figs. 1(a)–1(c); see also Xue *et al.*[40] where similar structures were found using Monte Carlo methods. Type I [Fig. 1(a)] consists of a classic vortex while type II is identified with two vortices and stripe domains [Fig. 1(b)]. This structure is closely related to the double-closure pattern with domain wall vertices as observed by McQuaid *et al.*[29] Type III is a more complicated pattern of domains forming a flux closure [Fig. 1(c)].

Having established three types of polarization patterns with vortex and stripe domains [Figs. 1(a)–1(c)] that can typically form on the cross-section of a nanowire, these patterns were studied further to establish the size dependency of their stability. Nanowire cross-sections of size 20–80 nm were simulated with initial conditions that forced each of the three patterns of Fig. 1 to form. This was achieved by initializing the simulation with the polarization at each node set to match one of the domain patterns in Fig. 1, while the nodal displacements and electric potential were initialized at zero. If the simulations reached equilibrium without pattern change, this indicated the stability of the pattern and the associated energy was thus found as a function of size. As the size was increased, the type I pattern remained stable, but other patterns became energetically favorable.

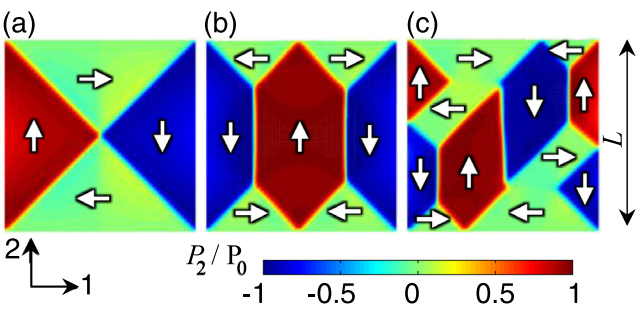

FIG. 1. Polarization, P_2, of the three patterns explored: (a) type I, (b) type II, and (c) type III. $P_0 = 0.26\,\text{C/m}^2$; $L = 40\,\text{nm}$.

The resulting free energy for each of the three types of polarization patterns obtained from the phase-field simulations is shown in Fig. 2(a) as a function of nanowire width, L. The energy per unit volume, ψ, is normalized as $(\psi_0 - \psi)/\psi_0$,[11] where ψ_0 corresponds to the energy per unit volume of a monodomain element in a spontaneously polarized state. The energy curves of type I and type II cross at $L \sim 34\,\text{nm}$, indicating a dependence of minimum energy state upon nanowire width. The type III pattern is not stable for $L < 35\,\text{nm}$: even if the simulation is started with polarization matching the type III pattern, other flux closures with lower energy form. The lower size limit for stability of the type III pattern is indicated by "A" in Fig. 2(a). Also shown in Fig. 2(a) are the results obtained from starting the simulations with randomly polarized states. These data jump back and forth between the main three types of polarization pattern indicating that the stable state found is highly dependent on the starting conditions.

Since the model size is much larger than the intrinsic length scale due to domain wall width, the total energy in volume V due to polarization gradient, $\int \psi_g dV$, scales approximately with domain wall area whereas domain energy, $\int \psi_d dV$, scales with the volume of polarized domains. Then, defining the total free energy $\psi_{\text{tot}} = \int \psi dV$, and defining the volume to have an out-of-plane depth D, the energy of a given pattern is

$$\psi_{\text{tot}} = aLD + bL^2D, \tag{5}$$

where the coefficients a and b for each pattern are estimated using linear regression of the data in Fig. 2(a), [see Fig. 2(b)].

For a given nanowire width, L, the gradient energy, ψ_g, of the three types of polarization patterns is governed by coefficient $a(\times 10^{16}\,\text{J/m}^2)$, which is related by type III > type II > type I. While ψ_d is governed by coefficient $b(\times 10^{24}\,\text{J/m}^3)$ and follows the reverse order type I > type II > type III. Thus, the multidomain patterns reduce their domain energy at the cost of increased gradient energy.

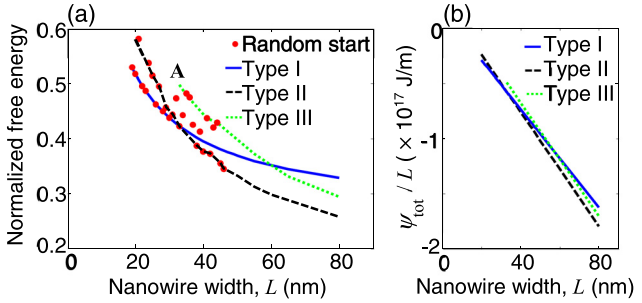

FIG. 2. (a) Normalized free energy, $(\psi_0 - \psi)/\psi_0$, values as a function of nanowire width for three types of polarization patterns obtained from phase-field simulations. (b) Total free energy per unit width, ψ_{tot}/L, versus L, showing best fit straight lines.

When $L < 34\,\text{nm}$, the percentage contribution of ψ_g to ψ is significant (25%–30%), causing polarization patterns with greater domain wall area to possess greater energy [Fig. 2(a)]. This makes the classic polarization vortex (type I) energetically favorable when $L < 34\,\text{nm}$. However, for $L > 50\,\text{nm}$, ψ_d dominates the energy. Thus, for $L > 50\,\text{nm}$, polarization patterns with stripe domains become favorable. The balance of energy contributions: ψ_g, ψ_d, and nanowire width, L, determines the minimum energy polarization pattern [Figs. 2(a) and 2(b), Eq. (5)]. Noting that the energy is well fitted by $\frac{\psi_{tot}}{L^2 D} = \frac{a}{L} + b$, then in the limit as L becomes large, $\frac{\psi_{tot}}{L^2 D} \to b$. Hence, the curves in Fig. 2(a) asymptotically approach a constant energy per unit volume. This suggests that the type III domain pattern will become favorable at larger scales. However, in the present study, calculations did not go beyond $L = 80\,\text{nm}$; it is likely that other low energy patterns will become favorable before the cross-over from type II to type III is reached.

Up to this point, surface energy was neglected and only open-circuit boundary conditions were considered. However, at the nanoscale, both surface energy, γ,[41–43] and electrical boundary conditions[36,44] affect the formation of ferroelectric domains. For $BaTiO_3$ nanowires, experiments and theoretical considerations suggest γ values of about 0.68 N/m;[36,44] however, the presence of depolarization field and surface layer effects can cause local variation in γ values and have led to greater estimates of γ, around 10 N/m.[44] Other authors found values within this range depending on shape and surface conditions including chemical environment.[42,43] Hence, we allow surface energy values in the range $0\,\text{N/m} \le \gamma \le 10\,\text{N/m}$ in the model. Morozovska *et al.*[45–47] have modelled the effect of a surface tension proportional to local curvature of cylindrical nanoparticles and nano-rods, via the free energy function. For our case involving a square cross-section nanowire we approximate the effect of surface tension by applying surface force boundary conditions at corners only, neglecting second order effects on surface curvature due to deformation. The surface effect on the Helmholtz free energy ψ in a narrow region near the nanowire surface is also neglected. Local polarization orientation relative to the surface also affects the value of γ, and indeed the relation between the surface energy and the resulting surface stresses is expected to be anisotropic. However, since this study focuses on flux closures, we expect polarization to be parallel to the surface and so neglect this effect. We further consider short- or open-circuit boundary conditions. A "phase diagram" mapping the minimum energy equilibrium state for each combination of γ and L, with open- and short-circuit boundary conditions is shown in Figs. 3(a) and 3(b). Boundaries on the diagram indicate approximately the location of points where the patterns associated with the adjacent regions have equal energy; markers show specific points calculated on each boundary.

In nanowire cross-section with open-circuit boundary conditions [Fig. 3(a)], type I polarization pattern is the minimum energy arrangement in a region with $10\,\text{nm} < L < 30\,\text{nm}$ approximately, and surface energy, $\gamma < 4\,\text{N/m}$. At greater values of surface energy, complex patterns with multiple domains are favored, while nanowire widths $L > 30\,\text{nm}$ favor the type II pattern as the lowest energy state. $BaTiO_3$ nanowires with open-circuit boundary condition are non-ferroelectric for combinations of high values of surface energy, $\gamma > 4\,\text{N/m}$ and low values of width, $L < 10\,\text{nm}$. This is manifested in the model by the disappearance of tetragonality ($\varepsilon_{11} = \varepsilon_{22} = 0$) and polarization $P_1 = P_2 = 0$. By contrast, in a nanowire with short-circuit boundary condition [Fig. 3(b)], a monodomain state is favored at low values of surface energy $\gamma < 2\,\text{N/m}$, when $L > 2\,\text{nm}$. There is a narrow region where polarization patterns with band-like domains and complex patterns with multiple domains are observed, with $10\,\text{nm} < L < 20\,\text{nm}$ and $\gamma > 4\,\text{N/m}$. Finally, the model suggests that $BaTiO_3$ nanowires with short-circuit boundary condition are non-ferroelectric when $\frac{\gamma}{L} > 8.5 \times 10^8\,\text{N/m}^2$.

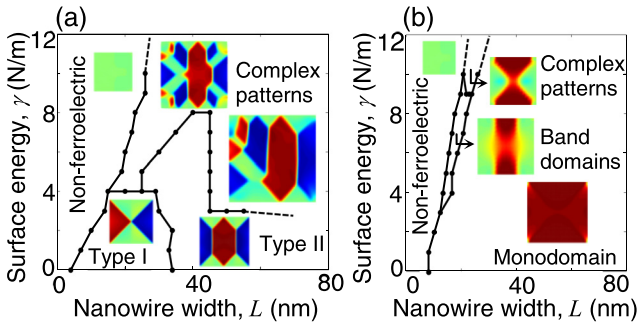

FIG. 3. Phase diagrams showing minimum energy domain patterns with (a) open-circuit boundary conditions and (b) short-circuit boundary conditions. Inset diagrams show typical patterns of polarization P_2/P_0.

The phase diagrams in Fig. 3 are consistent with several aspects of experimental observations. The lack of experimental observations of the classic (type I) polarization vortex is explained by two factors. First, scale effects are important in that typical experiments which map in-plane polarization patterns use sample sizes of order 100 nm upwards.[25,27,30,32] The simulations suggest that the type I vortex is a high energy state at this scale. Second, surface environments in experiments often include polar or ionic species that may act as charge carriers, providing some conductivity.[21,30,36,48,49] Again, the simulations suggest that the type I vortex is unlikely to form in conductive environments. Other features that agree with experiment include the loss of tetragonality at small scales; this has been observed in barium titanate nanowires at scales of 10 nm or less.[50–52] Meanwhile in nanowires with short-circuit boundary conditions, ferroelectricity has been observed down to the nanometer scale provided the surface energy is low, consistent with Fig. 3(b).[36] At greater length scales, 80 nm upward, complex domain patterns including several or many domains are typical.[25,27,32,48]

In conclusion, we used a phase-field simulation to study the effects of scale and surface conditions on the polarization patterns that can form in $BaTiO_3$ nanowires. There exists a narrow range of scale and surface conditions for which the classic single polarization vortex is likely to form. The study thus provides an insight into the absence of experimental observation of classic polarization vortices of the form described by Kittel: typical experiments in nanowires and nanoparticles do not operate in the regime where such vortices are energetically favorable. At scales on the order of a hundred nanometers, the classic single vortex is unlikely to

appear because of high domain energy, which is lowered in multiple domains. At smaller scales, ferroelectricity is plagued by surface energy and surface conductance that affect the formation of a single vortex, making it elusive.

The authors wish to thank Professor C. M. Landis and Dr. D. Carka for help in providing program codes and advice. They also acknowledge Dr. I. Münch for advice on modelling. A. Renuka Balakrishna gratefully acknowledges support of the Felix scholarship trust.

[1]C. Kittel, Phys. Rev. **70**, 965 (1946).
[2]T. Shinjo, T. Okuno, R. Hassdorf, K. Shigeto, and T. Ono, Science **289**, 930 (2000).
[3]A. Wachowiak, J. Wiebe, M. Bode, O. Pietzsch, M. Morgenstern, and R. Wiesendanger, Science **298**, 577 (2002).
[4]R. Skomski, J. Phys. Condens. Matter **15**, R841 (2003).
[5]J. Raabe, R. Pulwey, R. Sattler, T. Schweinböck, J. Zweck, and D. Weiss, J. Appl. Phys. **88**, 4437 (2000).
[6]A. Renuka Balakrishna, J. E. Huber, and C. M. Landis, Smart Mater. Struct. **23**, 085016 (2014).
[7]C. M. Wu, W. J. Chen, Y. Zheng, D. C. Ma, B. Wang, J. Y. Liu, and C. H. Woo, Sci. Rep. **4**, 3946 (2014).
[8]L. Hong and A. K. Soh, Mech. Mater. **43**, 342 (2011).
[9]N. Balke, B. Winchester, W. Ren, Y. H. Chu, A. N. Morozovska, E. A. Eliseev, M. Huijben, R. K. Vasudevan, P. Maksymovych, J. Britson, S. Jesse, I. Kornev, R. Ramesh, L. Bellaiche, L. Q. Chen, and S. V. Kalinin, Nat. Phys. **8**, 81 (2011).
[10]I. Naumov and H. Fu, Phys. Rev. Lett. **98**, 077603 (2007).
[11]I. Münch and J. E. Huber, Appl. Phys. Lett. **95**, 022913 (2009).
[12]S. Boyn, S. Girod, V. Garcia, S. Fusil, S. Xavier, C. Deranlot, H. Yamada, C. Carrétéro, E. Jacquet, M. Bibes, A. Barthélémy, and J. Grollier, Appl. Phys. Lett. **104**, 052909 (2014).
[13]P. C. Van Buskirk, J. F. Roeder, S. M. Bilodeau, M. W. Russell, S. T. Johnston, D. J. Vestyck, and T. H. Baum, U.S. Patent No. 7,705,382 (April 27, 2010).
[14]J. F. Scott, Science **315**, 954 (2007).
[15]J. Shieh, Y.-N. Lin, N.-T. Tsou, and Y.-C. Shu, Smart Mater. Struct. **22**, 094011 (2013).
[16]J. F. Scott, Europhys. Lett. **103**, 37001 (2013).
[17]D. Sichuga and L. Bellaiche, J. Phys. Condens. Matter **26**, 025302 (2014).
[18]A. Gruverman, D. Wu, H.-J. Fan, I. Vrejoiu, M. Alexe, R. J. Harrison, and J. F. Scott, J. Phys. Condens. Matter **20**, 342201 (2008).
[19]M. Dawber, K. M. Rabe, and J. F. Scott, Rev. Mod. Phys. **77**, 1083 (2005).
[20]G. D. Belletti, S. D. Dalosto, and S. Tinte, Phys. Rev. B **89**, 174104 (2014).
[21]R. Ahluwalia, N. Ng, A. Schilling, R. G. P. McQuaid, D. M. Evans, J. M. Gregg, D. J. Srolovitz, and J. F. Scott, Phys. Rev. Lett. **111**, 165702 (2013).
[22]L.-W. Chang, V. Nagarajan, J. F. Scott, and J. M. Gregg, Nano Lett. **13**, 2553 (2013).
[23]Y. Ivry, D. P. Chu, J. F. Scott, and C. Durkan, Phys. Rev. Lett. **104**, 207602 (2010).
[24]C.-L. Jia, K. W. Urban, M. Alexe, D. Hesse, and I. Vrejoiu, Science **331**, 1420 (2011).
[25]L. J. McGilly and J. M. Gregg, Nano Lett. **11**, 4490 (2011).
[26]L. J. McGilly and J. M. Gregg, Appl. Phys. Lett. **98**, 132902 (2011).
[27]L. J. McGilly, A. Schilling, and J. M. Gregg, Nano Lett. **10**, 4200 (2010).
[28]R. G. P. McQuaid, L. J. McGilly, P. Sharma, A. Gruverman, and J. M. Gregg, Nat. Commun. **2**, 404 (2011).
[29]R. G. P. McQuaid, A. Gruverman, J. F. Scott, and J. M. Gregg, Nano Lett. **14**, 4230 (2014).
[30]A. Schilling, D. Byrne, G. Catalan, K. G. Webber, Y. A. Genenko, G. S. Wu, J. F. Scott, and J. M. Gregg, Nano Lett. **9**, 3359 (2009).
[31]J. Wang, Appl. Phys. Lett. **97**, 192901 (2010).
[32]J. M. Gregg, Ferroelectrics **433**, 74 (2012).
[33]P. Aguado-Puente and J. Junquera, Phys. Rev. Lett. **100**, 177601 (2008).
[34]S. Ray, Y. V. Kolen'ko, D. Fu, R. Gallage, N. Sakamoto, T. Watanabe, M. Yoshimura, and M. Itoh, Small **2**, 1427 (2006).
[35]T. Hoshina, H. Kakemoto, T. Tsurumi, S. Wada, and M. Yashima, J. Appl. Phys. **99**, 054311 (2006).
[36]J. E. Spanier, A. M. Kolpak, J. J. Urban, I. Grinberg, L. Ouyang, W. S. Yun, A. M. Rappe, and H. Park, Nano Lett. **6**, 735 (2006).
[37]A. Kontsos and C. M. Landis, J. Appl. Mech. **77**, 041014 (2010).
[38]A. Kontsos and C. M. Landis, Int. J. Solids Struct. **46**, 1491 (2009).
[39]Y. Su and C. M. Landis, J. Mech. Phys. Solids **55**, 280 (2007).
[40]F. Xue, X. S. Gao, and J.-M. Liu, J. Appl. Phys. **106**, 114103 (2009).
[41]K. Uchino, E. Sadanaga, and T. Hirose, J. Am. Ceram. Soc. **72**, 1555 (1989).
[42]Y. Su, H. Chen, J. J. Li, A. K. Soh, and G. J. Weng, J. Appl. Phys. **110**, 084108 (2011).
[43]J. J. Wang, X. Q. Ma, Q. Li, J. Britson, and L.-Q. Chen, Acta Mater. **61**, 7591 (2013).
[44]W. Ma, Appl. Phys. A **96**, 915 (2009).
[45]A. N. Morozovska, E. A. Eliseev, and M. D. Glinchuk, Phys. Rev. B **73**, 214106 (2006).
[46]A. N. Morozovska, M. D. Glinchuk, and E. A. Eliseev, Phys. Rev. B **76**, 014102 (2007).
[47]M. D. Glinchuk, E. A. Eliseev, A. N. Morozovska, and R. Blinc, Phys. Rev. B **77**, 024106 (2008).
[48]A. Schilling, R. M. Bowman, G. Catalan, J. F. Scott, and J. M. Gregg, Nano Lett. **7**, 3787 (2007).
[49]A. Schilling, S. Prosandeev, R. G. P. McQuaid, L. Bellaiche, J. F. Scott, and J. M. Gregg, Phys. Rev. B **84**, 064110 (2011).
[50]W. S. Yun, J. J. Urban, Q. Gu, and H. Park, Nano Lett. **2**, 447 (2002).
[51]J. J. Urban, J. E. Spanier, L. Ouyang, W. S. Yun, and H. Park, Adv. Mater. **15**, 423 (2003).
[52]J. Hong and D. Fang, Appl. Phys. Lett. **92**, 012906 (2008).